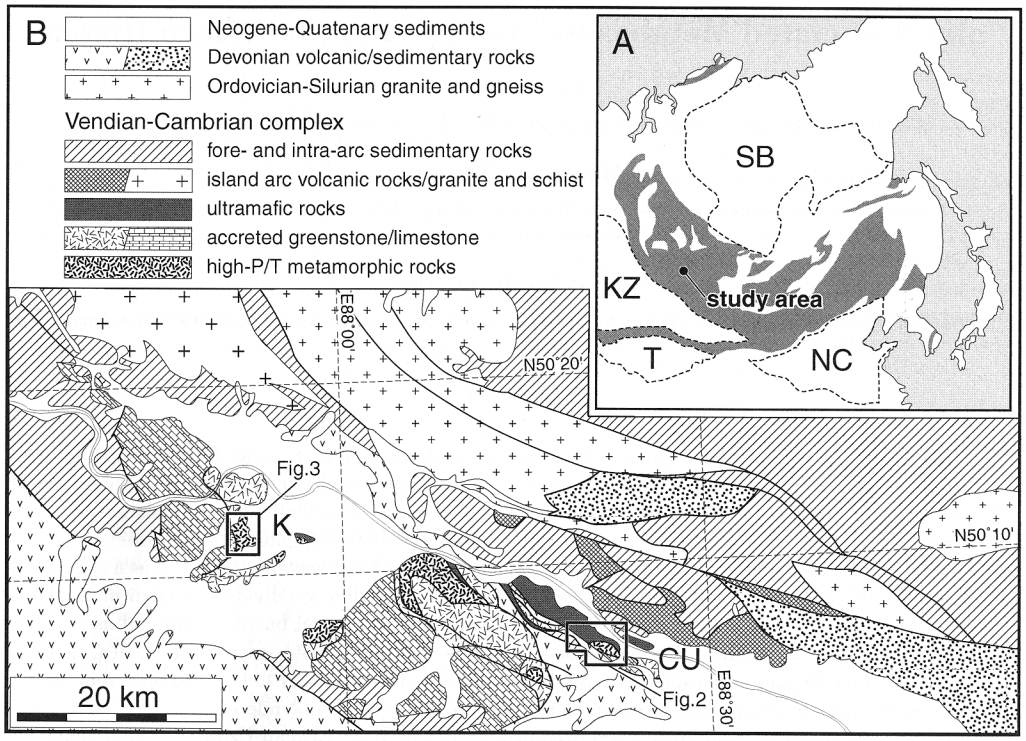

FIG. 1. A. Index map of Paleozoic orogens (grey) in the central Asian fold belt, surrounded by the Siberian (SB) and North China (NC) cratons, and Tarim (T) and Kazakhstan (KZ) blocks (modified after Sengör et al., 1994). B. Geological sketch map of the Kurai zone, Gorny Altai, southern Russia (simplified after Buslov et al., 1993). Thick lines show Late Paleozoic strike-slip and high-angle normal faults. Location of Figures 2 and 3 are also shown. Abbreviations: K = Kurai; CU = Chagan-Uzun.

Zonenshain et al., 1990, Berzin et al., 1994), parts of which have been subjected to HP/LT metamorphism related to oceanic plate subduction (Buslov et al., 1993; Buslov and Watanabe, 1996). These HP/LT metamorphic rocks have been briefly described, but their detailed mineralogical characteristics have not been analyzed.

Recent field mapping in the Chagan-Uzun and Kurai areas of the northern Altai Mountains was undertaken in order to investigate the eclogite, garnet-amphibolite, and lower-grade schists. The purpose of this paper is to describe the metamorphic petrology of these metabasites, and to discuss their P-T evolution and the paleo-geotherm of the Late Precambrian Altai subduction-zone.

Tectonic Setting and Geological Outline

The central Asian fold belt (between the Siberian and the North China cratons) and the Kazakhstan composite block contain Caledonian accretionary and collisional complexes (Fig. 1) (Zonenshain et al., 1990; Sengör et al., 1994; Dobretsov et al., 1995). The Gorny Altai region in southwestern Siberia, one of the best studied regions in the central Asian fold belt, consists of: (1) an accretionary complex with Vendian–Early Cambrian seamounts; (2) fragments of a Vendian–Early Cambrian boninite-tholeiitic island arc; and (3) a Cambrian calc-alkaline island arc with a forearc and intra-arc basin (Buslov et al., 1993; Simonov et al., 1994; Dobretsov et al., 1995; Berzin and Kungurtsev, 1996). In the Chagan-Uzun and Kurai areas in the southern part of the Gorny Altai region (Fig. 1), a Vendian–Early Cambrian accretionary complex extends northwest and southeast, and is overlain by the Vendian–Cambrian island arcs. An Ordovician–Silurian granite-gneiss dome intrudes the island arcs. Devonian volcanic and sedimentary rocks that formed in an active continental margin setting overlie the Ven-

dian–Cambrian complexes, and lastly several Late Paleozoic strike-slip faults and high-angle normal or reverse faults transect the entire structure (Buslov et al., 1993; 2001).

At Chagan-Uzun (Figs. 1B and 2), the Cambrian island-arc complex, the accretionary complex, and the Devonian sedimentary rocks are distributed, and between the two complexes, an ophiolitic and a HP/LT metamorphic complex are structurally intercalated. The island-arc complex consists of andesitic lava, acidic to intermediate tuffaceous rocks, limestone, mudstone, and minor sandstone. The accretionary complex consists of lower greenstones with limestone lenses, and upper limestones with greenstone lenses in a serpentinite matrix. The greenstone originated as clastic rock of basaltic composition and rarely contains cobble-sized fragments of basaltic lava. The bedded limestone typically contains cherty lens and layers. The ophiolitic complex is mostly composed of serpentinized dunite with pyroxenite dikes, massive amphibolite with a low-P type mineral assemblage (probably representing gabbro subjected to ocean-floor metamorphism), pillowed or massive basalts with intercalations of limestone, and dolerite dikes. The metamorphic complex consists of recrystallized serpentinite and antigorite schist, with intercalations of metabasites, and pelitic and calcareous schists. These intercalations are deformed or folded conformably with the enclosing antigorite schist. The metabasites include eclogite, garnet-amphibolite, amphibolite, and lower-grade basic schist. Sparse petrochemical data suggest that the eclogite and garnet-amphibolite have mid-ocean ridge basalt compositions (Buslov et al., 1993). K-Ar ages of the metabasites range from 535 to 567 Ma (Buslov and Watanabe, 1996), however, recent Ar-Ar ages from amphiboles in the eclogites show that most of the previous K-Ar data are mixed ages affected by later events, and that the Ar-Ar plateau age of ~630 Ma is a more reliable time constraint for the eclogite-related metamorphism (Buslov et al., 2001).

At Kurai (Figs. 1B and 3A), the accretionary complex and the metamorphic complex are juxtaposed along a high-angle normal fault. The accretionary complex is composed of greenstone and limestone; the greenstone is pillowed basalt and dolerite. The limestone is massive or bedded, and generally intercalated with the basaltic rocks. The metamorphic complex consists of metabasites with minor intercalations of siliceous and calcareous schists (Fig. 3A).

Field Occurrences of Metabasites

The Chagan-Uzun metabasites occur as lenses within the antigorite schist. They range from 1 m to 2 km across; the eclogites, garnet-amphibolites, and amphibolites tend to occur as smaller lenses in the lower structural level, whereas the lower-grade basic schists comprise the largest lens in the upper level. The eclogite is largely retrogressed into garnet-amphibolite along veins and its margins, and the eclogitic mineral assemblages only occur in lenses and layers a few to several centimeters thick. Garnet-amphibolite has three modes of occurrence: (1) retrogressed eclogite, mentioned above, which is generally massive, but partly sheared and veined. Chlorite-rich layers and dusty aggregates are developed on the shear planes and around the veins, respectively. (2) Intercalations less than 1 m thick within the eclogite body. These are foliated, contain abundant garnet porphyroblasts, and are veined and cut by the same shear planes as the eclogite, suggesting that formation of type-2 predated that of type-1. (3) Discrete intercalations within the antigorite schist, which are well foliated and associated with the pelitic and calcareous schists. Also, rare amphibolites occur as discrete lenses within the antigorite schist. A lower-grade basic schist (LBS) is generally associated with the calcareous schist, some of which is weakly foliated and preserves its igneous textures, suggesting that its protolith was a basaltic lava.

In contrast, the Kurai metabasites occur as a coherent body. Compared with the Chagan-Uzun metabasites, the Kurai metabasites are heterogeneously foliated, and characteristically preserve their igneous textures in low strain zones. These textures suggest that protoliths of the Kurai metabasites were basaltic lava and dolerite. The degree of recrystallization and grain size of the metabasalts vary with metamorphic grade, as indicated by their mineral assemblages, described later.

Petrography

Constituent minerals of the Chagan-Uzun and Kurai metabasites (about 400 samples) are summarized in Table 1. Hereafter, mineral abbreviations after Kretz (1983) are used except for the following: Amp = amphiboles; Bar = barroisite; Clin = clinochlore; Nam = sodic amphibole; Phn = phengite; Win = winchite.

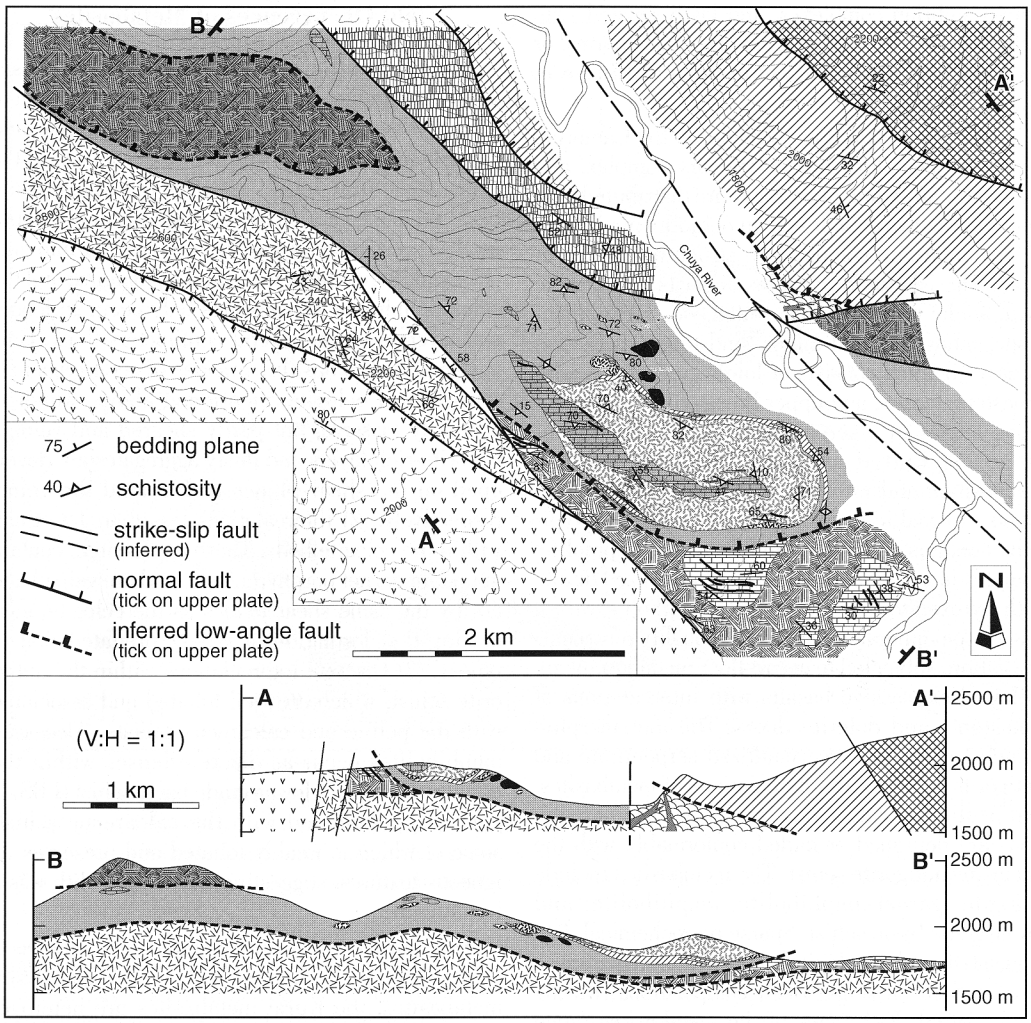

Devonian volcanic and clastic rocks

Vendian-Cambrian complexes

island arc complex

andesitic lava

tuffaceous rocks, limestone, mudstone and sandstone

Ophiolitic complex

basaltic lava with dolerite dike

amphibolite

peridotite/serpentinite

Metamorphic complex

serpentine (antigorite) schist

eclogite (partly amphibolitized)

garnet-amphibolite

basic schist

pelitic schist

calcareous schist

Accretionary complex

basaltic lava and clastic rocks

limestone with cherty lens or layer

FIG. 2. Geologic map and cross-sections of the Chagan-Uzun area.

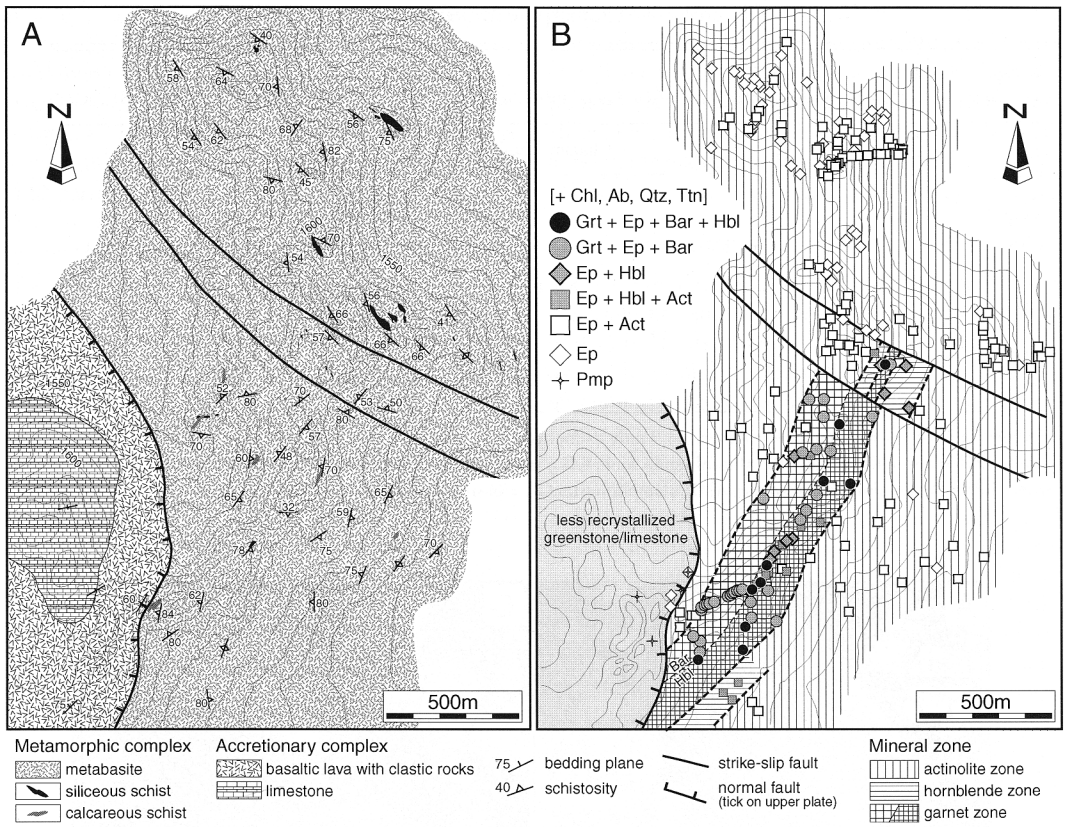

FIG. 3. Geologic map (A) and metamorphic mineral zones (B) of the Kurai area.

Chagan-Uzun metabasites

The Chagan-Uzun eclogites are characterized by an assemblage of Grt + Omp + Bar + Ep + Qtz + Rt. In general, they are granoblastic, but preferred orientations of barroisite, epidote, and omphacite form weak foliations that are cut by Prh + Qtz or Ep + Cal + Qtz veinlets. Subhedral garnets range from 0.5 to 8 mm in diameter, and coarse-grained ones are replaced by chlorite and stilpnomelane along fractures and margins. They contain abundant inclusions of epidote, barroisite, quartz, omphacite, rutile, albite, and phengite. The last two minerals only occur as inclusions in the garnets, and form composite inclusions with barroisite. Omphacites form pale-green subhedral crystals with long axes up to 5 mm in length. They are replaced by actinolite along cracks and rims, and are typically surrounded by radial aggregates of stilpnomelane needles. Blue-green barroisites are generally porphyroblastic and frequently mantled by pale blue glaucophane, which is further rimmed by actinolite (Fig. 4A). Rarely, glaucophane occurs between barroisite and omphacite grains, where it is in direct contact with—or is separated from—the omphacite by a film of actinolite (Fig. 4B). Some glaucophanes occur as subhedral crystals within cracks of garnet porphyroblasts, and they are rimmed by barroisite at the contact with garnet (Fig. 4C). Rutiles occur in the matrix and as inclusions in garnet and barroisite; matrix rutiles are rimmed by titanite.

Garnet-amphibolites commonly contain Grt + Bar + Ep + Ttn, with minor quartz, albite, phengite, rutile, winchite, and chlorite; barroisite and rutile are generally rimmed by actinolite and titanite, respectively. Type-1 garnet-amphibolite mainly consists of Bar + Grt + Ep, and contains dusty aggregates of Act + Stp + Chl with or without albite, probably after omphacite, near Prh + Qtz and Ep + Cal + Qtz veins. This type contains minor quartz in the matrix. Barroisites are coarse grained, and show

TABLE 1. Summary of Metamorphic Minerals in Metabasites[1]

Rock type/zone	Act	Hbl	Win	Bar	Rbk	Gln	Grt	Omp	Prh	Pmp	Ep	Ab	Qtz	Phn	Chl	Ttn	Ilm	Rt	Cal
									Chagan-Uzun										
EC	–			++		+	++	++	–		++	(+)	++	(+)	–	–		++	–
GA	–		+	++		+	++		–		++	+	+	+	+	++		+	+
AMP		++							–		+	++	+		–	+		+	
LBS	+				+					+	+	++	++	+	++	++			++
									Kurai										
GH	+	++		++			++		–		++	++	++	+	+	+	+	+	–
GB	+	+		++			++		–		++	++	++	+	+	+	+		+
HBL	+	++									++	++	++	+	++	++	+		+
ACT	++										++	++	++	++	++	++			++

[1]Abbreviations: ++ = common; + = minor; (+) = only as inclusion in garnet; – = only as secondary occurrence of minerals; ACT = actinolite zone; HBL = hornblende zone; GB = garnet-barroisite subzone; GH = garnet-hornblende subzone; LBS = lower-grade basic schist; AMP = amphibolite; GA = garnet-amphibolite; EC = eclogite.

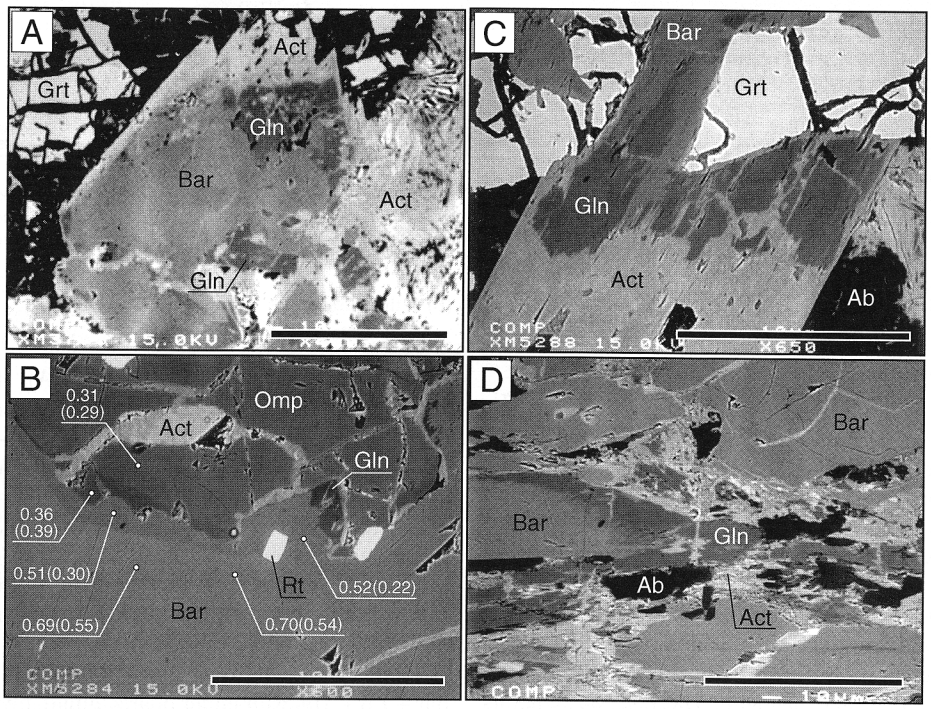

FIG. 4. Backscattered images of amphiboles in eclogite (A–C) and garnet-amphibolite (D) from Chagan-Uzun. Scale bars are 0.1 mm. A. Barroisite porphyroblast, patchily replaced by glaucophane. The outermost margins are rimmed by actinolite. B. Contact between amphibole and omphacite, where barroisite and glaucophane are in direct contact with omphacite, and are partly rimmed by actinolite. Numbers and those in parentheses indicate Fe^{2+}/Mg ratios and Xjd in omphacite, and edenite mol% in barroisite. C. Contact between amphibole and garnet, where glaucophane is rimmed by barroisite at the contact with garnet and is associated with actinolite overgrowths. D. Porphyroblastic barroisites (grey), mantled by glaucophane (dark grey). Along margins and cracks, both barroisite and glaucophane are replaced by actinolite (light grey).

sub- or anhedral shapes. Garnets are subhedral and fractured. Around the shear planes, they are chloritized along the margins, giving rise to chloritic layers. Epidotes tend to be prismatic in domains rich in barroisite. The type-2 garnet-amphibolite, intercalated within the eclogite, is characterized by abundant garnet porphyroblasts and by the absence of albite and quartz in the matrix. Schistosity is formed by the preferred orientation of elongated barroisite and prismatic epidote. Garnets occur as euhedral crystals, ranging from 0.5 to 1.5 mm in diameter, and contain inclusions of quartz, barroisite, and stilpnomelane. Titanites form tiny crystals in the schistosity or replace rutile. Type-3 garnet-amphibolite is highly foliated and contains porphyroblastic garnet, elongated barroisite and epidote, chlorite and phengite flakes, and lenticular albite porphyroblasts. Subhedral or euhedral garnets are up to 0.5 mm in size, and contain inclusions of barroisite, epidote, rutile, and quartz; these inclusions form folded trails continuous with the matrix schistosity. Many garnets are cut by quartz veins, and chloritized along their margins. Barroisites are rimmed by glaucophane like those in the eclogites, and both barroisite and glaucophane are replaced by actinolite along cracks and margins (Fig. 4D). Rare winchites occur as small flakes together with epidote and barroisite in the matrix.

The amphibolites are medium grained and heterogeneously foliated. They have an assemblage of Hbl + Ab + Qtz + Ttn with or without epidote. Pale-green or green hornblendes are porphyroblastic with long axes up to 2 mm in length, and their grain boundaries are filled with albite and minor quartz. Granular or prismatic titanites typically form clusters in the matrix. Fine-grained prismatic epidotes are mostly included in albite. Rare rutiles are mantled by titanites. Some quartz veins with calcite or prehnite cut the foliation, where hornblendes are chloritized.

The LBS are less thoroughly recrystallized than other rock types and in general contain colorless clinopyroxene as a relict igneous mineral. Mineral assemblages in the LBS are: Act + Chl + Pmp + Stp, Pmp + Chl + Phn, Ep + Chl, and Rbk + Act + Chl, with quartz, albite, and titanite. Actinolites generally form colorless acicular crystals with chlorite in the matrix. Riebeckites form violet or pale purple, small prisms or acicular crystals, which are generally associated with actinolite but never coexist with pumpellyite and epidote. Pumpellyites occurs as colorless or pale yellow, tiny laths in the albite-rich domains and as vein minerals with irregular shapes. Ubiquitous chlorites occur as aggregates with irregular shapes or as flakes with actinolite, riebeckite, pumpellyite, and epidote in the matrix. Quartz, albite, calcite, titanite, and rare hematite are scattered in the matrix; the first three predominate in the veins.

Kurai metabasites

The Kurai metabasites include metabasalt and metadolerite, and their degrees of recrystallization and grain sizes vary according to their mineral assemblages and protoliths. Based on their mineral assemblages, the metabasites are divided into three major mineral zones: actinolite, hornblende, and garnet (Fig. 3B). In general, zone boundaries are parallel to the foliation of the metabasites. The actinolite zone (ACT) is in the northern, western, and southeastern parts of the area, and the garnet zone is in the central part where it has a maximum width of 250 m; the 50 to 150 m wide hornblende zone (HBL) occurs between the above two zones. The garnet zone can be subdivided into a garnet-barroisite subzone (GB) in the west and garnet-hornblende subzone (GH) in the east. As a whole, the degrees of recrystallization and grain size of the metabasites increase with metamorphic grade from the ACT through the HBL and the GB to the GH.

The ACT metabasites have an assemblage of Ep + Act + Chl + Ab + Qtz + Ttn + Cal with or without phengite and hematite, and tend to lack actinolite in the north. They are generally fine-grained and show a weak schistosity formed by acicular actinolites with chlorite. Ubiquitous epidote, titanite, albite, and quartz are scattered in the matrix. Rare porphyroblastic actinolites contain tiny inclusions of titanite.

The HBL metabasites consist of Ep + Hbl + Act + Chl + Ab + Qtz + Ttn, characteristically including calcite, phengite, and ilmenite. The rocks are fine-grained but generally foliated; amphiboles, epidote, and chlorite define the schistosity. Pale green hornblende and actinolite occur as discrete acicular or prismatic grains, but some hornblendes are rimmed by actinolite. Epidote and titanite are granular or prismatic, and relatively coarser grained than those in the ACT metabasites.

GB metabasites are characterized by an assemblage of Grt + Ep + Bar + Ab + Chl + Ttn + Qtz with or without hornblende and actinolite. They rarely contain Ep + Chl + Ab + Qtz + Ilm, with either hornblende or actinolite or both, near the boundary with

the ACT. The GB metabasites are well foliated, and barroisite and epidote form a stretching mineral lineation. Garnets are subhedral or euhedral, less than 1 mm in size, and include quartz, epidote, and titanite. They are associated with quartz, prismatic epidote, and platy chlorite in pressure shadows. Blue-green barroisites are prismatic or porphyroblastic with long axes up to 2 mm in length, and are associated with chlorite, titanite, and phengite. The elongated barroisites tend to be replaced by actinolite at their margins. In some samples, the matrix contains minor calcite, albite, and quartz. Textures and constituents in the garnet-free samples are mostly similar those in the HBL metabasites. In some metabasites, Ep + Cal + Qtz or Prh + Qtz veinlets cut the schistosity.

GH metabasites contain the assemblages Grt + Ep + Bar + Hbl + Ab + Chl + Qtz + Ttn, Grt + Ep + Bar + Ab + Chl + Qtz + Ttn with or without rutile, and Ep + Hbl + Chl + Ab + Qtz + Ilm with or without actinolite. Garnet-bearing metabasites are generally gneissose, but micro-folding and related axial planar cleavages are developed in well-foliated samples. Garnet porphyroblasts range from 1 to 5 mm in diameter, and include abundant hornblende, epidote, quartz, and titanite. They are often replaced by pale chlorite along their margins. Blue-green barroisites define the foliations together with prismatic epidote, porphyroblastic albite, chlorite, and titanite. In the garnet-bearing metabasites, hornblendes occur as pale green to green discrete, lenticular or prismatic grains. Both barroisite and hornblende are often rimmed by actinolite, and replaced by pale chlorite along axial planar cleavages. The foliation of the GH metabasites is cut by Prh + Qtz veins, and calcite occurs only as a vein mineral. Garnet-free samples exhibit similar textures to those in the HBL.

Metadolerites occur in all mineral zones, and commonly contain relict clinopyroxene phenocrysts, brown or brownish green hornblende, magnetite, and irregular epidote. Relic minerals in the ACT are replaced by chlorite, titanite, epidote and actinolite. However in higher-grade zones, pale-green hornblende, actinolite, chlorite and epidote not only replace relic minerals, but also occur as matrix constituents.

Mineral Chemistry

Mineral compositions were analyzed using a JEOL JXA8800 electron microprobe analyzer at the Department of Earth and Planetary Sciences, Tokyo Institute of Technology. Analytical conditions were: accelerating voltage of 15 kV, specimen current 12 nA on Faraday cup, and beam diameter 1–5 μm. X-ray intensities were reduced using an oxide ZAF matrix correction scheme. Table 2 shows representative mineral analyses for the metabasites.

Amphiboles

Structural formulae and Fe^{3+} contents in amphiboles were calculated on the assumption: Si + Al + Ti + Fe + Mn + Mg = 13 for O = 23. Compositions of analyzed amphiboles are shown in Figure 5. Glaucophane (Xgln), magnesioriebeckite (Xmrb), actinolite (Xact), and tschermakite (Xts) components were calculated as $Al^{VI}/(Al^{VI} + Fe^{3+}) \times Na/(Ca + Na)[B]$, $Fe^{3+}/(Al^{VI} + Fe^{3+}) \times Na/(Ca + Na)[B]$, $(Si-6)/2 \times Ca/(Ca + Na)[B]$ and $(8-Si)/2 \times Ca/(Ca + Na)[B]$, respectively. Nomenclature of amphiboles and their end-member formulae are after Leake et al. (1997).

In the Chagan-Uzun metabasites, glaucophanes (Xgln = 0.65–0.91) have $Fe^{2+}/(Fe^{2+} + Mg)$ of 0.30–0.48 in the eclogites and of 0.23–0.32 in the garnet-amphibolites. Riebeckites in the LBS yield Xgln of 0.29–0.46 and $Fe^{2+}/(Fe^{2+} + Mg)$ of 0.47–0.65. Barroisites and winchites have Xgln of 0.17–0.43 and 0.26–0.29, and $Fe^{2+}/(Fe^{2+} + Mg)$ of 0.21–0.42 and 0.26–0.29, respectively, and show variations between glaucophane and actinolite with Xmrb less than 0.21. The barroisites are rich in (Na + K)[A] up to 0.55 (O = 23). Barroisites from the glaucophane-bearing eclogites and garnet-amphibolites (type 3) are relatively low in Xts, whereas those from the type-2 garnet-amphibolite are slightly low in Xgln and $Fe^{2+}/(Fe^{2+} + Mg)$. As described before, both barroisite and glaucophane in the eclogites are in direct contact with omphacite (Fig. 4B), where barroisite is poor in Fe^{2+}/Mg, (Na + K)[A] and Xts, compared with its mantle to core domains. Barroisites replacing glaucophane at the contact with garnet exhibit lower (Na + K)[A] and Xts than those mantled by glaucophane. In type-3 garnet-amphibolites, barroisites rarely retain compositions of actinolitic hornblende in their cores. Hornblendes and actinolites range in $Fe^{2+}/(Fe^{2+} + Mg)$ from 0.23 to 0.37 and from 0.30 to 0.66, respectively. A compositional gap between the riebeckites and associated actinolites is comparable with that in pumpellyite-actinolite facies metabasites (Toriumi, 1975).

In the Kurai area, the metadolerites generally contain relict brown hornblende, which is pargasitic and higher in Ti (up to 0.28 for O = 23) than the

TABLE 2. Representative Mineral Analyses of Metabasites[1]

Rock type:	EC						GA					AMP		LBS						
Mineral:	Bar	Gln	Act	Omp	Grt	Ep	Bar	Gln	Grt	Ep	Chl	Hbl	Ab	Pmp (v)	Chl	Mrb	Chl	Act	Pmp	Chl
SiO_2	49.91	57.43	53.97	55.02	38.14	37.94	48.68	56.38	37.97	38.35	27.22	51.46	67.70	37.15	27.49	54.19	26.88	53.05	36.96	25.59
TiO_2	0.17	0.06	0.04	0.06	–	0.12	0.30	0.10	0.08	0.12	–	0.21	0.01	0.02	–	0.01	–	0.08	0.04	–
Al_2O_3	11.19	11.69	0.57	8.71	21.67	26.67	11.33	11.51	21.67	26.46	16.69	5.87	19.67	25.21	17.57	3.26	18.39	0.57	25.27	19.50
FeO*	14.54	11.78	17.73	7.99	26.89	7.33	13.28	10.96	27.31	7.95	30.59	10.77	0.22	3.54	24.67	20.14	25.90	15.69	3.32	29.35
MnO	0.03	–	0.32	–	0.13	0.02	0.02	0.06	0.25	0.05	0.43	0.27	0.06	0.43	0.39	0.17	0.41	0.25	0.72	0.49
MgO	10.25	9.21	12.10	7.68	3.69	0.04	11.27	10.41	2.77	0.03	12.03	15.21	–	2.70	15.44	8.33	13.55	12.72	2.32	11.77
CaO	7.38	0.99	11.84	13.40	9.25	23.29	7.58	1.85	10.37	23.73	0.26	11.91	0.79	22.01	0.12	2.81	0.03	11.87	21.52	–
Na_2O	4.03	7.12	0.36	6.25	–	–	4.15	6.25	0.04	0.02	0.02	0.88	10.38	0.05	0.01	5.40	0.02	0.26	0.13	0.01
K_2O	0.30	0.01	0.14	0.04	–	0.01	0.33	0.05	–	0.01	0.02	0.03	0.08	–	0.01	0.03	–	0.01	0.02	–
Total	97.78	98.28	97.06	99.14	99.77	95.43	96.93	97.56	100.47	96.71	87.26	96.60	98.91	91.10	85.69	94.33	85.17	94.50	90.29	86.71
O=	23	23	23	6	12	12.5	23	23	12	12.5	14	23	8	24.5	14	23	14	23	24.5	14
Si	7.154	7.872	7.991	2.001	2.999	3.012	7.018	7.736	2.979	3.012	2.974	7.396	2.984	6.072	2.957	8.057	2.928	8.001	6.090	2.796
Al	1.891	1.889	0.099	0.373	2.008	2.495	1.924	1.861	2.004	2.449	2.149	0.995	1.022	4.856	2.228	0.571	2.361	0.101	4.908	2.511
Ti	0.018	0.007	0.004	0.002	–	0.007	0.032	0.010	0.005	0.007	–	0.022	0.000	0.003	–	0.001	–	0.009	0.005	0.000
Fe_{3+}	0.325	0.170	0.027	0.064	0.000	0.486	0.412	0.430	0.035	0.522	–	0.250	0.008	0.010	–	0.855	–	0.000	0.000	–
Fe_{2+}	1.417	1.180	2.168	0.179	1.769	–	1.190	0.828	1.757	–	2.795	1.044		0.474	2.219	1.648	2.360	1.979	0.458	2.681
Mn	0.003	–	0.040	–	0.01	0.001	0.003	0.007	0.017	0.003	0.039	0.033	0.002	0.059	0.035	0.021	0.037	0.032	0.101	0.046
Mg	2.191	1.882	2.671	0.417	0.433	0.005	2.421	2.129	0.324	0.004	1.960	3.260	–	0.658	2.476	1.846	2.200	2.860	0.569	1.916
Ca	1.133	0.145	1.878	0.522	0.779	1.981	1.172	0.273	0.872	1.997	0.031	1.834	0.037	3.853	0.014	0.447	0.004	1.919	3.799	–
Na	1.119	1.891	0.103	0.441	–	–	1.160	1.662	0.007	0.003	0.004	0.244	0.887	0.015	0.001	1.558	0.004	0.075	0.042	0.001
K	0.054	0.002	0.026	0.002	–	0.001	0.060	0.009	–	0.001	0.003	0.006	0.004	–	0.001	0.006	–	0.001	0.003	–

Zone	GH					GH (Grt-free)				GB					HBL			ACT		
Mineral:	Bar	Grt	Ep	Chl	Ab	Hbl (R)	Hbl	Ep	Chl	Bar	Grt	Ep	Chl	Phn	Hbl	Ep	Chl	Act	Ep	Chl
SiO_2	44.93	38.05	37.71	25.21	67.71	45.64	44.55	37.03	25.49	47.81	38.47	38.61	26.87	50.49	44.35	37.02	25.06	55.63	38.17	26.12
TiO_2	0.45	0.06	0.10	0.05	0.08	2.09	0.32	0.03	0.07	0.21	0.14	0.01	0.08	0.14	0.23	0.14	0.05	0.05	–	0.01
Al_2O_3	13.77	21.45	27.34	20.26	18.81	8.11	10.89	23.75	19.67	11.69	21.69	25.84	19.81	29.22	9.88	23.69	20.34	0.66	25.26	19.87
FeO*	15.47	26.91	6.60	28.28	0.21	19.30	21.20	10.70	29.45	14.29	27.13	8.86	24.80	2.61	19.77	11.07	28.15	13.48	9.75	25.94
MnO	0.05	0.90	0.07	0.17	–	0.37	0.30	0.15	0.41	0.10	1.58	0.05	0.13	–	0.31	0.18	0.30	0.17	0.18	0.36
MgO	9.04	2.41	0.05	13.17	–	8.09	7.21	0.02	10.55	10.27	1.72	0.00	15.77	2.77	8.13	0.03	12.48	15.48	0.03	14.96
CaO	9.67	10.02	23.51	–	0.27	11.61	10.15	23.03	0.11	8.28	10.45	23.67	0.02	–	10.45	22.99	0.06	12.59	23.47	0.04
Na_2O	1.85	–	0.01	–	11.56	1.06	1.66	0.02	0.04	3.34	0.04	0.03	–	0.65	1.92	0.02	–	0.13	0.02	0.05
K_2O	0.10	–	0.01	–	0.01	0.22	0.18	–	0.03	0.16	–	–	0.01	10.06	0.22	–	–	–	0.01	–
Total	95.33	99.80	95.40	87.12	98.64	96.47	96.46	94.72	85.82	96.15	101.22	97.06	87.48	95.95	95.27	95.13	86.43	98.20	96.89	87.34
O=	23	12	12.5	14	8	23	23	12.5	14	23	12	12.5	14	11	23	12.5	14	23	12.5	14
Si	6.640	3.010	2.992	2.721	3.000	6.957	6.707	2.998	2.816	6.977	3.011	3.027	2.822	3.341	6.776	2.988	2.728	7.952	3.009	2.775
Al	2.399	2.000	2.557	2.577	0.982	1.457	1.932	2.267	2.561	2.010	2.000	2.387	2.453	2.279	1.780	2.254	2.609	0.112	2.346	2.488
Ti	0.050	0.003	0.006	0.004	0.003	0.239	0.036	0.002	0.006	0.023	0.008	0.000	0.007	0.007	0.027	0.009	0.004	0.006	–	0.001
Fe_{3+}	0.609	0.000	0.438	–	0.008	0.003	0.787	0.725	–	0.426	–	0.581	–	–	0.579	0.747	–	0.080	0.642	–
Fe_{2+}	1.303	1.780	–	2.552	–	2.457	1.883	–	2.721	1.318	1.776	–	2.179	0.144	1.948	–	2.562	1.531	–	2.305
Mn	0.006	0.060	0.005	0.016	–	0.048	0.038	0.010	0.038	0.012	0.105	0.003	0.011	–	0.040	0.012	0.028	0.020	0.012	0.032
Mg	1.992	0.285	0.006	2.118	–	1.838	1.617	0.002	1.738	2.233	0.200	0.000	2.470	0.273	1.851	0.003	2.025	3.299	0.003	2.370
Ca	1.531	0.849	1.999	–	0.013	1.896	1.637	1.998	0.013	1.295	0.877	1.988	0.002	–	1.712	1.988	0.007	1.928	1.982	0.004
Na	0.531	–	0.001	–	0.993	0.313	0.485	0.003	0.008	0.944	0.005	0.004	–	0.084	0.570	0.003	–	0.036	0.004	0.011
K	0.019	–	0.001	–	0.000	0.042	0.035	–	0.005	0.030	–	–	0.001	0.849	0.043	–	–	–	0.001	–

[1]See text for calculations of the amount of ferric iron in minerals. Abbreviations:—= not detected; FeO* = total iron as FeO; R = relic; v = in vein. Other abbreviations are the same as listed in Table 1.

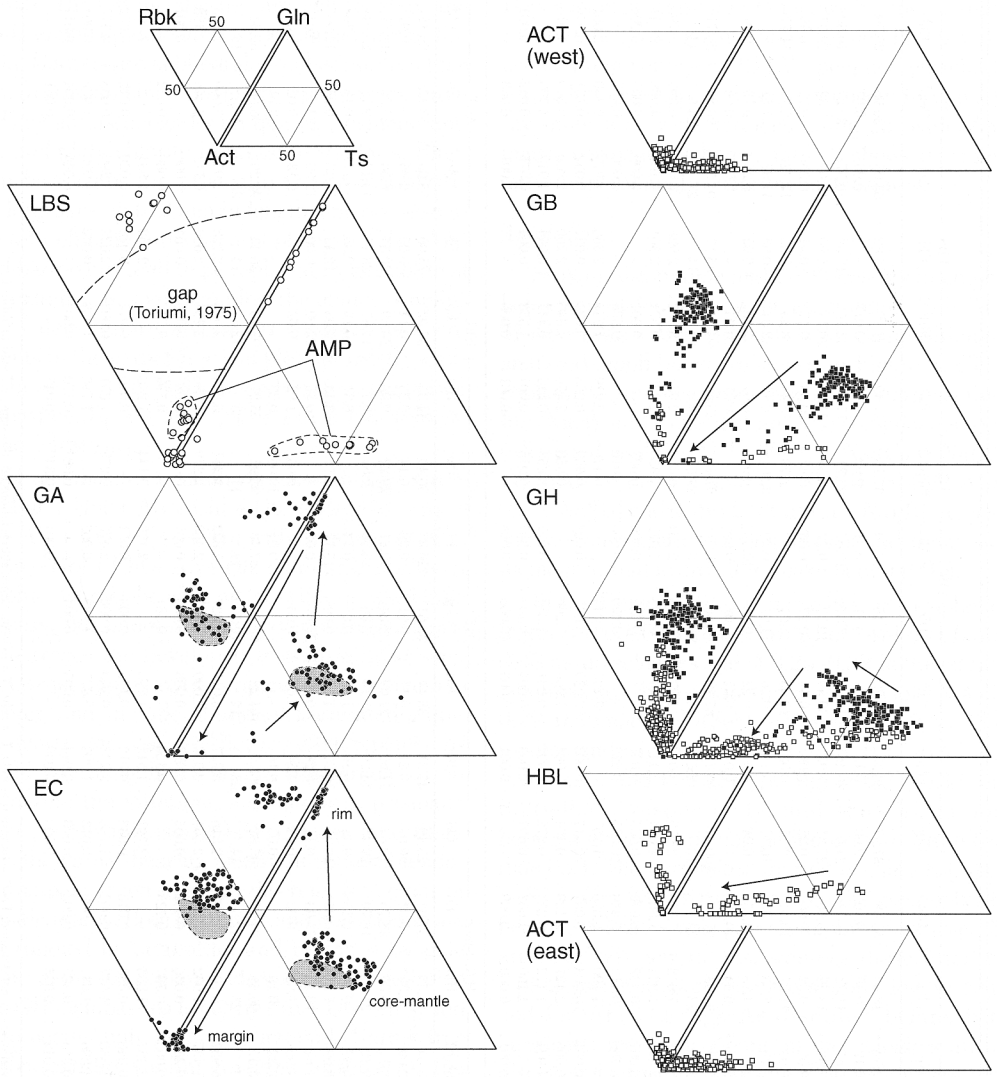

FIG. 5. Glaucophane-riebeckite-actinolite and glaucophane-tschermakite-actinolite triangular ternary diagrams, showing compositional variations of amphiboles in Chagan-Uzun (left) and Kurai (right) metabasites. A compositional gap between sodic and calcic amphiboles in pumpellyite-actinolite facies metabasites (Toriumi, 1975) is also shown. Solid and open symbols indicate garnet-bearing and -free metabasites, respectively. Light-shaded fields indicate compositional range of garnets from type-2 garnet-amphibolite. Arrows indicate trends of compositional change of zoned amphiboles. Abbreviations are the same as those used in Table 1.

green hornblende. The composition of the relict hornblende is comparable with that of amphibole in gabbroic rocks subjected to hydrothermal alteration in the ocean floor (e.g., Gaggero and Cortesogno, 1997; Werner, 1997).

On the other hand, regional metamorphic amphiboles systematically change in composition according to their mineral assemblage or zone. In garnet-free metabasites, amphiboles vary from actinolite in the ACT to magnesiohornblende and hornblende in the HBL, GB, and GH. Their $Fe^{2+}/(Fe^{2+} + Mg)$ increase from 0.24 to 0.60 with increasing Xts and (Na + K)[A] (up to 0.49). Some hornblendes are retrogressively zoned to actinolite in their rims.

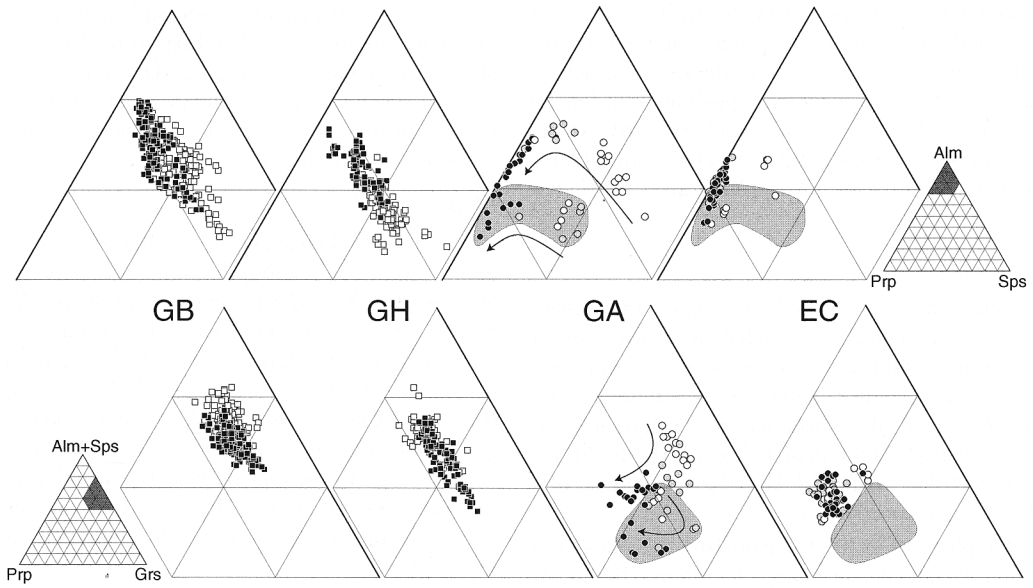

FIG. 6. Almandine-pyrope-spessartine (above) and (almandine + spessartine)–pyrope–grossular (below) ternary diagrams showing compositional variations of garnets in metabasites. Light-shaded fields indicate compositional range of garnets from type-2 garnet-amphibolite. Solid and open symbols show rim and mantle-core compositions, respectively, and arrows indicate compositional change of highly zoned garnets. Abbreviations are the same as those used in Table 1. See text for further explanations.

Amphiboles in the garnet-bearing metabasites are classified as actinolite, magnesiohornblende, and barroisite in the GB, whereas in the GH they also contain minor tschermakite, edenite, and pargasite with (Na + K)[A] up to 0.63, but lack actinolite. Their $Fe^{2+}/(Fe^{2+} + Mg)$ ratios range from 0.30 to 0.51; barroisites are slightly higher in $Fe^{2+}/(Fe^{2+} + Mg)$. Calcic amphiboles in the matrix of the garnet-bearing metabasites contain Xgln up to 0.24, but those as the inclusions in garnets in the GH metabasites are magnesiohornblende with lower Xgln. The barroisites contain Xmrb up to 0.20, and those from the GB are slightly enriched in both Xgln and Xmrb; values of (Xgln + Xmrb) reach 0.46 in the GB and 0.34 in the GH. Barroisite porphyroblasts are typically rimmed by actinolite, and some have zoned cores of magnesiohornblende with higher Xts.

As a whole, amphiboles from the Kurai metabasites systematically increase in Xts and (Na+K)[A] from the ACT in the west and the east toward the GH in the central part of the area. The Xgln shows a similar trend, but amphiboles with the highest Xgln occur in the GB.

Garnet

Stoichiometry and Fe^{3+} content of garnet were calculated based on eight cations and charge balance constraints (O = 12). Analyzed garnets are almandine with Fe^{3+}/(total Fe) less than 0.05. Their compositions can be expressed by the four components of almandine (Xalm), pyrope (Xprp), spessartine (Xsps), and grossular (Xgrs).

Garnets tend to be richer in Xprp with increasing metamorphic grades (Fig. 6); the Xprp are 0.03–0.09 in the GB metabasites and 0.05–0.16 in the garnet-amphibolites. The Xgrs ranges from 0.24 to 0.37; the maximum Xgrs slightly increases from 0.33 in the GB to 0.37 in the type-2 garnet-amphibolite. Garnets in the eclogites are rich in Xprp (0.09-0.16), and their Xgrs shows less variation, 0.25–0.30.

In the Kurai metabasites, compositional variations in individual garnets are controlled by decreasing Xsps with increasing Xgrs and Xalm toward the rims. Garnets from the GB preserve progressive zoning with slight increase of Xprp towards the rims, whereas those from the GH have mostly homogeneous Xprp. In the Chagan-Uzun garnet-

amphibolites, the Xsps decrease with increases of Xgrs and Xalm, and the Xprp significantly increases with a decrease of Xgrs toward the rims. Garnets in the eclogites show fewer compositional variations but generally preserve cores rich in Xsps. At the outermost margins, most garnets show retrogressive zoning with decreasing Xprp, Xgrs, and $Fe^{2+}/(Fe^{2+}+$ g).

Omphacite

Structural formulae and Fe^{3+} content in omphacite were calculated by charge balance constraints for six oxygens, and their compositions are expressed by four components: jadeite (Xjd), acmite (Xacm), augite (= diopside + hedenbergite: Xaug), and Ca-Tschermak (Xcats) calculated as $(Al^{VI}-Al^{IV})/(Ca + Na)$, $Fe^{3+}/(Ca + Na)$, $(Ca\text{-}Al^{IV})/(Ca + Na)$, and $Al^{IV}/(Ca + Na)$, respectively.

Omphacites in the Chagan-Uzun eclogites contain trace amounts of Xcats—less than 0.02 (rarely up to 0.04). Their Xjd, Xacm, and $Fe^{2+}/(Fe^{2+} + Mg)$ range from 0.27 to 0.46, 0.02 to 0.10, and 0.17 to 0.51, respectively. Symplectitic omphacites with albite contain a maximum Xjd of 0.45.

Some analyzed omphacites preserve progressive normal zoning, but most show reverse zoning with decreases of both $Fe^{2+}/(Fe^{2+} + Mg)$ and Xjd at the margins. Rarely, the omphacites exhibit normal zoning with significant increases of $Fe^{2+}/(Fe^{2+} + Mg)$ and Xjd to the contact with barroisite; however, at the contact with glaucophane, there is little variation in omphacite composition (Fig. 4B).

Ca-Al hydrosilicates

Epidotes contain a pistacite component (Xps = $Fe^{3+}/(Fe^{3+} + Al)$) from 0.11 to 0.30, which broadly decreases with increasing metamorphic grade. The Xps is also controlled by local bulk-rock compositions; epidotes replacing igneous plagioclases in the LBS and the ACT metabasites, and those included in albite from the amphibolites are distinctively lower in Xps (0.11–0.15). However, epidote inclusions in garnet porphyroblasts are relatively high in Xps (0.16–0.26). Epidotes have rims with higher and lower Xps in the Chagan-Uzun and Kurai metabasites, respectively.

Pumpellyites in metabasites are rich in Al (Table 2), depending on bulk compositions in domains with pumpellyites, such as veins and layers composed mainly of albite and quartz. Their Fe^{3+} contents are negligible, and Al/(Al + total Fe + Mg) and $Fe^{2+}/(Fe^{2+} + Mg)$ ratios range from 0.80 to 0.83 and 0.42 to 0.63, respectively, where the stoichiometry and Fe^{3+} contents were calculated based on 16 cations and charge balance constraints (O = 24.5). Prehnites in secondary veins contain Fe_2O_3 of 0.6–2.6 wt%, with total iron as ferric, and normally have cores relatively rich in Fe.

Chlorite

Chlorites in the metabasites yield wide compositional variations according to mineral assemblages and samples. For garnet-free metabasites, Al/(Al + Si) and Fe/(Fe + Mg) of chlorites range from 0.43 to 0.50 and 0.38 to 0.63, respectively. Chlorites in garnet-bearing metabasites range in Al/(Al + Si) from 0.45 to 0.49, and in Fe/(Fe + Mg) from 0.41 to 0.58. As a whole, chlorites with higher Fe/(Fe + Mg) are characteristic in the higher-grade GH metabasites, whereas those with lower Al/(Al + Si) are predominant in the riebeckite-bearing or the amphibole-free LBS (Fig. 7).

Phengite

Phengites in the metabasites show Si values from 3.30 to 3.45 (O = 11), which are higher in the lower-grade metabasites, and increase with $Fe^{2+}/(Fe^{2+} + Mg)$ (0.24–0.42). The Na/(Na + K) ratios range from 0.09 to 0.12 in the higher-grade metabasites, and are higher than those in the lower-grade metabasites, commonly less than 0.02.

Albite

Albites have anorthite contents (Xan = Ca/(Ca + Na + K)) less than 0.02, and exhibit slightly higher Xan up to 0.04 in Chagan-Uzun amphibolites and Kurai GH metabasites.

Geothermometry

In this study, the following conventional geothermometers were used; Fe^{2+}-Mg partitioning of garnet-clinopyroxene calibrated by Berman et al. (1995) and Krogh Ravna (2000), and of garnet-hornblende by Graham and Powell (1984). In order to obtain equilibrium temperatures at peak metamorphism, in cases where minerals exhibit normal zoning, rim compositions were used. For grains with reverse zoning, compositions were selected from mantles to cores with higher Mg/Fe^{2+} and Xgrs for garnets, higher Fe^{2+}/Mg and Xjd for omphacites, and higher Fe^{2+}/Mg for amphiboles.

In highly retrogressed eclogites, garnets exhibit lower Mg/Fe^{2+}, and omphacites tend to be low in Fe^{2+}/Mg and Xjd, compared with those in less retro-

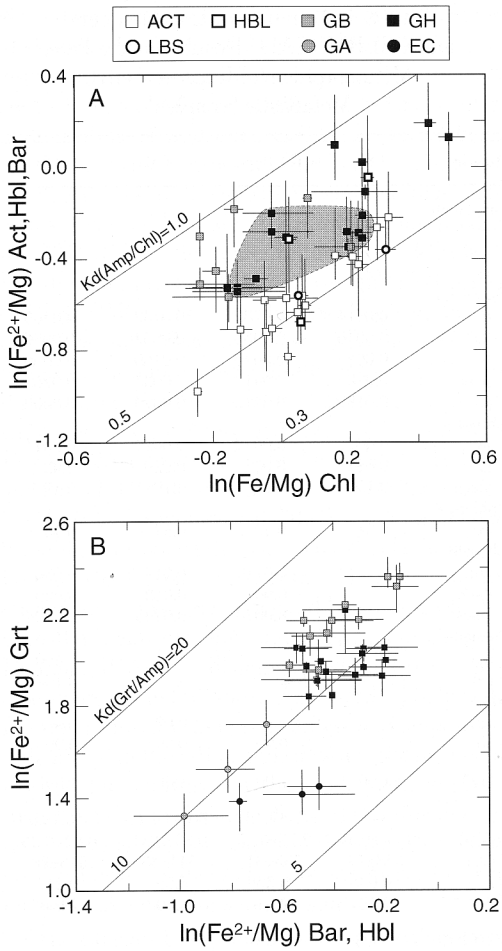

FIG. 7. Fe-Mg partitioning between chlorite and amphiboles (A), and between amphiboles and garnet (B) in metabasites. Each plot with a bar shows a mean value with dispersion of selected mineral compositions within each sample. A light-shaded field indicates compositional range of amphibole-chlorite pairs in garnet-bearing metabasites from the garnet-hornblende subzone. Abbreviations are the same as those used in Table 1.

gressed eclogites. Therefore, garnet-omphacite pairs for the thermometric calculations were selected from the least retrogressed eclogite.

For garnet-clinopyroxene thermometry of eclogites, there is a serious problem regarding omphacite compositions; omphacites with higher Xjd contents yield apparently higher T estimates (e.g., Hirajima, 1996). For the Chagan-Uzun eclogites, T estimates using the calibration of Berman et al. (1995) do not yield a significant correlation with the Xjd, whereas those of Krogh Ravna (2000) obviously increase with increasing Xjd, so that the estimates by these two calibrations yield differences up to 80°C at 1.5 GPa. The estimates using the calibration of Berman et al. (1995), 600–640°C at 1.5 GPa and 620–660°C at 2.0 GPa, were taken as the peak T conditions for the Chagan-Uzun eclogites. Application of the garnet-hornblende thermometer to garnet-barroisite pairs coexisting with omphacites yielded T estimates of 600–640°C, in good agreement with the estimates by the garnet-clinopyroxene thermometer.

For the Chagan-Uzun garnet-amphibolites, compositions of garnets and barroisites in the type-2 and type-3 garnet-amphibolites yielded T estimates of 570–610°C and of 470–560°C, respectively. In the Kurai metabasites, garnets coexist with both barroisite and hornblende. With the mineral pairs selected according to the criteria noted above, calculated temperatures using the garnet-hornblende thermometer did not show a significant variation among the different amphibole species. Thus, the calculated values from the two kinds of amphiboles are not distinguished hereafter.

The garnet-hornblende thermometer for the GB metabasites yielded T estimates of 491 ± 45°C, which is an average value with two-sigma errors for 11 samples, where 3 to 32 mineral pairs were used for the calculation in each sample; the maximum dispersion in temperature was 70°C within one sample. Taking the dispersion in each sample into account, the T differences by samples are mostly negligible. On the other hand, garnet-amphibole pairs from the GH metabasites gave values of 551 ± 61°C for 10 samples. In each sample, 3 to 28 mineral pairs yielded the maximum dispersion of 80°C. As a result, the estimated temperatures for the GB are lower than those for the GH metabasites, although their differences are not substantial.

Discussion

Metamorphic peak conditions

The application of conventional geothermometers provided T estimates of the peak metamorphism for the high-grade metabasites; however, further thermobarometry required combination of experimentally or thermodynamically reliable reactions and computed petrogenetic grids in the basaltic Na_2O–CaO–MgO–Al_2O_3–SiO_2–H_2O (NCMASH) system (Yokoyama et al, 1986; Liou et al., 1987; Evans, 1990; Frey et al., 1991; Oh and Liou, 1998). Additionally, average P-T conditions were calcu-

TABLE 3. Independent Equilibria Used in THERMOCALC Calculations[1]

1: 3tr + 2py + 4gr = 12di + 3ts

2: 2di + 2ts + q = tr + py + 2cz

3: 3di + alm = 3hed + py

4: 5tr + 2parg + 6py + 12cz = 12di + 2jd + 13ts

5: 15hed + 19ts = 15di + 3fact + 14py + 16cz + 8H2O

6: 3gl + 2py + 4gr = 6di + 6jd + 3ts

7: 19ts = 3tr + 14py + 16cz + 8H2O

8: 82py + 27tr + 144cz + 12clin = 16gr + 147ts

9: 82py + 33tr + 144cz + 12ames = 16gr + 153ts

10: 4gr + 9ts + 6q = 4py + 3tr + 12cz

11: 2clin + 4ab = 2gl + ames + 2H2O

12: 15tr + 12parg + 22py + 72cz = 57ts + 6gl + 28gr

13: 74gr + 25alm + 18daph + 147q = 33fact + 78cz

14: 4gr + 15ts + 12an = 10py + 3tr + 24cz

15: 8gl + 5ames + 4q = 3py + 16ab + 7clin

16: 3tr + 3ts + 6parg + 18ab = 4py + 8gr + 12gl

17: 4gr + 5alm + 6cz + 15q = 3fact + 18an

18: 40gl + 9daph + 25ames + 20q = 15alm + 44clin + 80ab

19: 24gl + 35alm + 15ames + 12q = 44py + 21daph + 48ab

20: 6parg + 11py + 36cz + 57cel = 21tr + 3gl + 14gr + 57mu

[1]Formulae and abbreviations of end members are after Holland and Powell (1998).

TABLE 4. Activities of End Members and THERMOCALC Results for the Peak Metamorphism of Representative Metabasite Samples[1]

Activity	EC	GA (type3)	GH	GB
Omphacite				
di	0.39			
hed	0.17			
jd	0.37			
Barroisite				
tr	0.0274	0.0788	0.0138	0.0469
fact	0.0040	0.0034	0.0054	0.0056
ts	0.0029	0.0020	0.0160	0.0050
parg	0.0186	0.0410	0.0033	0.0205
gl	0.0189	0.0212	0.0090	0.0200
Garnet				
py	0.0071	0.0042	0.0029	0.0011
gr	0.024	0.032	0.029	0.029
alm	0.19	0.18	0.19	0.19
Epidote				
cz	0.51	0.48	0.57	0.45
Chlorite				
clin		0.011	0.017	0.036
daph		0.060	0.042	0.020
ames		0.0070	0.0205	0.0304
Phengite				
mu				0.460
cel				0.104
Albite				
an		n.c.	0.02	n.c.
ab		0.99	0.99	0.99
H_2O	1.00	1.00	1.00	1.00
n.e.	1-7	7-13,18	7-10,13-17	7-13,19,20
P(GPa)	1.64±0.37	0.77±0.25	0.83±0.31	0.82±0.26
T (°C)	658±77	555±31	544±43	545±38
cor	0.035	0.238	0.25	0.217
sigfit	2.28	2.54	3.50	2.90
B95T (°C)	628			
GP84T (°C)	602	523	547	477

[1]Activities of end members were calculated using mineral compositions listed in Table 2. Abbreviations: n.c. = not used for calculation due to very small values; n.e. = numbers of independent equilibria calculated by THERMOCALC, listed in Table 3; cor = correlation between the uncertainties on P and T; sigfit = a goodness-of-fit parameter describing the averaging of equilibria (Powell and Holland, 1994); B95T = a temperature at 1.6 GPa estimated using the Berman et al. (1995)'s thermometer; GP84T, temperatures estimated using Graham and Powell's (1984) thermometer. Other abbreviations are the same as those used in Tables 1 and 3.

lated using an updated version of the internally consistent thermodynamic dataset and the computer program THERMOCALC version 3.1 (Powell and Holland, 1994; Holland and Powell, 1998). Mineral end-member activities were calculated for amphibole and chlorite following Dale et al. (2000) and Holland et al. (1998), respectively, and for clinopyroxene, garnet, epidote, phengite, and albite following Holland and Powell (1998). Quartz was assumed to be pure. Tables 3 and 4 show independent equilibria used in the THERMOCALC calculations, and the end-member activities and calculated average P-T conditions for peak metamorphism of representative metabasite samples.

The average T conditions computed using the THERMOCALC program are consistent with T estimates by the conventional thermometers, taking uncertainties into account, although the THERMOCALC results have relatively large uncertainties and most of their *sigfit* values are over statistical limits (Powell and Holland, 1994). However, only for the GB metabasite, the T condition determined using the THERMOCALC program yielded an obviously higher value than that by the conventional thermometer (Table 4). The cause of such a discrepancy may be differences in estimation of Fe^{3+} contents for amphiboles and numbers of components in

the system, and an incompatibility between the thermodynamic dataset and the calibration in the conventional thermometer. In this study, the Fe^{3+} contents for amphiboles were calculated as the maximum estimates, and were used in the garnet-hornblende thermometer calculation. In contrast, average values for the maximum and minimum estimates, required by Dale et al. (2000), were used in the THERMOCALC calculations. In addition, a K_2O-bearing phase, phengite, was included within the THERMOCALC calculations, but only for the GB metabasite. However, these differences yielded insignificant temperature differences of ~10°C. For the updated thermodynamic dataset used in this study, the entropy of ferroactinolite was raised by 30 J/mol, relative to the value in the dataset of Holland and Powell (1998), in order to correlate the garnet-hornblende thermometer and the natural Fe-Mg partitioning data among the phases used in Holland and Powell (1998) (Dale et al., 2000). However, why the entropy of ferroactinolite should be so much higher than the usual entropy summation methods (e.g., Holland, 1989) is still unresolved, and may cause discrepancies in this study. As described below, the Fe-Mg partitioning between garnets and amphiboles indicates that the GB metabasites are lower in equilibrium temperatures at the peak metamorphism than the GH metabasites. Thus, the estimated values by using the conventional thermometer, based on the Fe-Mg partitioning, are taken as the peak temperature conditions in this study.

The Chagan-Uzun eclogites are intercalated with the type-2 garnet-amphibolites, which contain garnets and barroisites with lower $Fe^{2+}/(Fe^{2+} + Mg)$. Because reaction curves around boundaries between the blueschist, epidote-amphibolite, and eclogite facies shift toward higher P-T sides with decreasing $Fe^{2+}/(Fe^{2+} + Mg)$ of the system (e.g., Evans, 1990; Oh and Liou, 1998), both the type-2 garnet-amphibolites and the eclogites could have formed under identical P-T conditions, corresponding to the eclogite facies. In common basaltic compositions, barroisitic amphiboles are stable up to 2.2 GPa at 650°C (Poli, 1993). However, the stability limit of clinopyroxene-free garnet-amphibolite is less than 2.0 GPa at 600°C and 1.8 GPa at 700°C (Liu et al., 1996), indicating that peak P conditions of the eclogites must be below 2.0–1.8 GPa at 600–700°C. The symplectite assemblage of Omp (Xjd = 0.45) + Ab without quartz yielded about 1.3 GPa at 590°C using the sliding equilibria of Jd + Qtz = Ab, as calculated by the THERMOCALC program. This value would give a maximum estimate of the minimum P conditions for the eclogites. The stability limit of antigorite (660°C at 2.0 GPa; Wunder and Schreyer, 1997) in the antigorite schists surrounding the eclogites defines the maximum T conditions for the eclogites. Integrating the THERMOCALC results, the possible peak conditions of the eclogites would be 590–660°C at 1.3–2.0 GPa.

The Chagan-Uzun garnet-amphibolites and the Kurai GB and GH metabasites have Grt + Ep + Bar + Ab + Ttn + Qtz as the common assemblage, which is characteristic of the high-P part of the epidote-amphibolite facies. Type-2 garnet-amphibolites are intercalated within the eclogites and contain no albite in their matrix; thus their possible peak P condition would be comparable to that of the eclogites. Type-3 garnet-amphibolites and the GB and GH metabasites predominantly contain rutile and ilmenite, respectively, suggesting that P-T conditions of the garnet-amphibolites are higher in dP/dT than those of the GB and GH metabasites, based on the stability relations of Ti-phases in the basaltic system (e.g., Ernst and Liu, 1998). The mineral assemblage in the GH metabasites, including hornblendes rich in (Na + K)[A] and Xts, represents conditions of the univariant reactions of Bar = Ed + Grt_{ss} (Prp-Grs solid solution) + Czo + Ab + Qtz + H_2O bounded by the low-T part, and of Czo + Clin + Ab + Qtz = Ed + Grt_{ss} + H_2O by the low-P part from the higher P-T part of the epidote-amphibolite facies. Moreover, they often contain albite slightly enriched in Xan, indicating that P-T conditions of the GH metabasites are close to the boundary between the high-P part of epidote-amphibolite and amphibolite facies, shown by a reaction of Czo + Grt_{ss} + Ab + Qtz = An + Ed + H_2O. These relations suggest that the metamorphic conditions of the GH metabasites exhibit the lowest dP/dT among the garnet-bearing metabasites, consistent with the results from the thermobarometric calculations.

The Chagan-Uzun amphibolites, and the Kurai HBL and ACT metabasites have assemblages of Hbl ± Ep, Hbl + Act + Ep + Chl ± Ilm ± Cal, and Act + Ep + Chl + Cal, respectively; all three contain Qtz + Ab + Ttn. The first two assemblages suggest conditions between the greenschist and the low-P part of the epidote-amphibolite facies, which are bounded by reactions such as Tr + Ab = Ed + Qtz and Tr + Clin + Czo + Qtz = Ts + H_2O. ACT metabasites contain a typical greenschist facies assemblage. The presence of a common Xan-rich albite in the Chagan-Uzun amphibolites suggests that metamorphic conditions

TABLE 5. Summary of Estimated Metamorphic Conditions of Metabasites[1]

Rock type/zone	Prograde stage	Peak stage	Retrograde stages	
			Early	Late	Latest
Chagan-Uzun					
EC	540-570°C/0.9-1.6GPa	590-660°C/1.3-2.0GPa	570°C/1.3-1.6GPa		
GA	– type2:	570-610°C/1.3-2.0GPa	–	270-380°C/0.3-0.8GPa	<280°C/0.2GPa
	– type3:	470-560°C/0.7-1.0GPa	–		
AMP	–	380-510°C/0.3-0.8GPa	–		
LBS	–	300-350°C/0.4-0.8GPa	–	–	–
Kurai					
GH	–	490-610°C/0.7-1.1GPa	–		
GB	–	450-540°C/0.7-1.1GPa	–	270-380°C/0.3-0.8GPa	<280°C/0.2GPa
HBL	–	370-440°C/0.3-0.9GPa	–		
ACT	–	270-380°C/0.3-0.8GPa	–		

[1]See text for details. Abbreviations are the same as in Table 1.

of the amphibolites are close to the transition between the low-P part of the epidote-amphibolite and amphibolite facies, represented by the reaction Czo + Clin + Qtz = An + Tr + H_2O or Czo + Clin + Ab + Qtz = An + Ed + H_2O.

The LBS contain high-variance assemblages of Fe^{3+}-poor Pmp + Act + Chl and Rbk + Act + Chl with albite, quartz, and titanite; the amphiboles do not coexist with epidote and hematite. These assemblages are common in the pumpellyite-actinolite facies, bounded by the reaction of Pmp + Clin + Qtz = Tr + Czo + H_2O from greenschist facies conditions. Decreasing (Fe^{2+} + Fe^{3+}) contents of the minerals shift this boundary reaction to the high-T side, up to 350°C at 0.5 GPa (Liou et al., 1987); therefore the P-T ranges of the LBS with Fe^{3+}-poor pumpellyites may partly overlap in temperature with those of the ACT metabasites with epidotes rich in Xps. The occurrence of riebeckite constrains the minimum P conditions for the LBS (0.4 GPa at 300–350°C; Maresch, 1977). Antigorite, derived from breakdown of chrysotile (around 300°C at 0.5 GPa; Evans et al., 1976), in the surrounding antigorite schist could provide the minimum T conditions.

Accordingly, the Chagan-Uzun and Kurai metabasites exhibit a wide P-T range with progressively increasing P-T conditions, from 0.4 GPa at 300°C to 2.0 GPa at 660°C, corresponding to the pumpellyite-actinolite, greenschist, epidote-amphibolite, and finally quartz-eclogite facies; the estimated P-T ranges are summarized in Table 5. This suggests that the metabasites in the Chagan-Uzun and Kurai areas belong to the metamorphic facies series of HP/LT intermediate type.

Thermal structure

Various mineral assemblages in the Chagan-Uzun and Kurai metabasites indicate their different P-T conditions, bounded by discontinuous reactions. Changes in the metamorphic grade, especially in temperature, can also be expressed by continuous reactions for sliding Fe^{2+}/Mg equilibria in coexisting minerals with identical mineral assemblages. In general, with an increase in metamorphic grade, coexisting amphibole and chlorite in metabasites with Ep + Ab + Qtz tend to increase Fe^{2+}/Mg ratios; however the production of garnet, which favors high Fe^{2+}/Mg, causes the Fe^{2+}/Mg ratios of coexisting minerals to decrease with increasing grade. In the studied metabasites, Fe^{2+}-Mg partitioning between amphiboles and chlorite, and between garnets and amphiboles vary as shown in Figure 7.

In the Kurai ACT, HBL, GB, and GH metabasites without garnet, the Fe^{2+}/Mg in amphiboles (actinolite, hornblende, and barroisite) and chlorites yield a positive correlation. The Fe^{2+}-Mg partition coefficients between amphiboles and chlorite ($Kd_{Amp/Chl} = (Fe^{2+}/Mg)_{amphiboles}/(Fe^{2+}/Mg)_{chlorite}$) systematically increase from 0.43–0.58 in the ACT, through 0.48–0.73 in the HBL and GB, to 0.66–0.94 in the GH metabasites (Fig. 7A). Actinolites and chlorites in the LBS coexist with pumpellyite instead of epidote, but the $Kd_{Amp/Chl}$ values are included in the range of the ACT metabasites. In metabasites with garnets, the Fe^{2+}/Mg in amphiboles and chlorite are lower than those in the garnet-free metabasites from identical mineral zones, and are plotted in a range slightly off the general trend (Fig. 7A). Their higher $Kd_{Amp/Chl}$ values of 0.57–0.94 exhibit no significant difference between the GB and the GH metabasites, because equilibrium temperatures in these zones are high enough to homogenize gradients in Fe^{2+}/Mg between amphiboles and chlorite.

On the other hand, the Fe^{2+}-Mg partitioning between garnet and amphiboles (hornblende and barroisite) shows changes in metamorphic grade among the high-grade metabasites, as shown by the results of garnet-hornblende thermometry. The Fe^{2+}/Mg in garnets systematically decreases with that in amphiboles, and the partition coefficients ($Kd_{Grt/Amp} = (Fe^{2+}/Mg)_{garnet}/(Fe^{2+}/Mg)_{amphiboles}$) continuously increase from 8.6–11.9 in the garnet-amphibolites, through 8.3–14.4 in the GH, to 10.8–15.2 in the GB (Fig. 7B). Eclogites with omphacite having low-Fe^{2+}/Mg contain barroisites with higher Fe^{2+}/Mg than those in the garnet-amphibolites, but the coexisting minerals yield the lowest $Kd_{Grt/Amp}$ of 6.3–9.0.

As a result, the Fe^{2+}-Mg partitioning between the coexisting minerals shows that the Chagan-Uzun and Kurai metabasites continuously increase in temperature from the lowest to the highest grades. In the Kurai area, the mineral zoning from the ACT to the GH yields a temperature range of about 300°C within less than 1 km width (Table 5 and Fig. 3). It is too narrow to detect changing the temperature within each mineral zone, but the Fe^{2+}-Mg partitioning between coexisting minerals indicates that the Kurai metabasites constitute a successive thermal structure from the ACT in the margins to the GH in the central part of the area.

P-T history

Textural relations and compositional changes of minerals in the high-grade metabasites from Chagan-Uzun and Kurai enable us to divide the metamorphism into several stages. In particular, the Chagan-Uzun eclogites have preserved prograde, peak, and retrograde stages, and the last can be subdivided into early, late, and latest substages.

As described above, garnet porphyroblasts in the eclogites include epidote, barroisite, quartz, omphacite, rutile, albite, and phengite; the last two minerals occur only as inclusions in garnets, and form composite inclusions with barroisite. These relations indicate that the garnets grew during the prograde to peak stages of metamorphism, and that the prograde stage can be characterized by the inclusion assemblage of Ab + Phn + Bar in garnet. Compositions of the inclusion minerals and adjacent garnet core yielded 540–570°C by the garnet-hornblende thermometer. Taking the stability of albite into account, the maximum P conditions of this stage are about 1.6 GPa.

Chemical zoning of diagnostic minerals in the high-grade metabasites also allows us to evaluate the progressive P-T changes. The normal zoning of garnet, with decreases of Xsps and Fe^{2+}/Mg toward the rims, is rather common in the high-grade metabasites except for the eclogites (Fig. 6), although omphacite and barroisite in the eclogites preserve their progressive chemical zoning.

Near the contact between omphacite and barroisite, the omphacite increases in Xjd and Fe^{2+}/Mg, whereas the barroisite decreases in (Na+K)[A], Xts, and Fe^{2+}/Mg towards the contact (Fig. 4B). This relation can be expressed by the following reaction:

$$\text{Ed (in Bar)} + 3\text{Qtz} = \text{Jd (in Omp)} + \text{Tr (in Bar)}. \quad (1)$$

Thermodynamic calculations and recent experimental studies indicate that edenite end-member isopleths have a positive slope in the Jd + Qtz stability in P-T space, and that the edenite components decrease with increasing dP/dT (Poli, 1993; Tropper et al., 2000). Compositional changes of the above two minerals indicate that their equilibrium temperatures increase with increasing metamorphic dP/dT, suggesting that the eclogites reached the peak stage conditions through a P-T path with a steeper dP/dT than the edenite isopleths. However, where glaucophane is intercalated between omphacite and barroisite grains, the omphacite does not show significant compositional changes. This relation suggests that edenite components were consumed to produce glaucophane instead of the jadeite components by the substitutions $Na^{[A]}Al^{IV}[]^{[A]}{}_{-1}Si_{-1}$ and

$Na^{[B]}Al^{VI}Ca^{[B]}_{-1}Mg_{-1}$, which can be expressed as follows:

$$2Ed\ (in\ Bar) + 6Qtz = Gln + Tr\ (in\ Bar) + 2Di\ (in\ Omp). \quad (2)$$

Assuming that reaction (2) occurred contemporaneously with reaction (1), glaucophane can be regarded as a prograde product during increasing metamorphic dP/dT. However, rare glaucophanes in cracks of garnet porphyroblasts imply that they were products of the retrograde stage accompanying deformation of the garnet porphyroblasts. These glaucophanes are replaced by barroisites along their contacts with garnets (Fig. 4C). This mode of occurrence can be expressed by the following hydration reaction:

$$Gln + 2Prp + Grs + Ab + Qtz + 2H_2O = 3Bar. \quad (3)$$

Reaction (3) indicates P-T conditions at the boundaries among the blueschist, epidote-amphibolite, and eclogite facies. Integrating the garnet-hornblende thermometry with the barroisite in contact with the garnet, estimated P-T conditions at this early substage of retrograde metamorphism are ~570°C at P conditions within the albite stability field. The retrograde path related to this substage would have passed through P-T ranges with slightly higher dP/dT than those of the prograde-stage metamorphism, and the glaucophanes would have formed at a period between the metamorphic peak stage and the early substage of retrograde metamorphism by hydration. Glaucophane formation by reaction (2) predates the extensive retrogression by hydration, but may have been affected by local differences in fluid activity, as reaction (2) is apparently balanced by the H_2O budget between glaucophane and barroisite.

Further retrogression formed actinolite overgrowths with albite along the margins of both barroisite and glaucophane. Some barroisites are patchily replaced by glaucophane prior to the actinolite overgrowths (Fig. 4A). Such textural relations of these amphiboles can be explained by the following reactions in the NCMASH system (Yokoyama et al., 1986):

$$12Bar + 2Ab + 10\ H_2O = 6Czo + 7Gln + 3Clin + Qtz, \quad (4)$$

$$6Czo + 25Gln + 7Qtz + 14H_2O = 6Tr + 9Clin + 50Ab, \quad (5)$$

$$50Bar + 58H_2O = 18Czo + 7Tr + 23Clin + 50Ab + 21Qtz. \quad (6)$$

Reactions (4), (5), and (6) define boundaries between the low-T part of the epidote-amphibolite and blueschist facies, between the blueschist and greenschist facies, and the low-T part of the epidote-amphibolite and greenschist facies. Barroisites with glaucophane patches and actinolite rims were formed by passing through reaction (4) followed by reaction (5) with a decrease of both P and T, whereas the replacements of glaucophane and barroisite by actinolite would take place under decreasing P-T conditions across reactions (5) and (6), respectively. In P-T space, the invariant point from which these univariant reactions radiate shifts toward low-P and low-T sides by introducing Fe_2O_3 and FeO in the system, respectively (Yokoyama et al., 1986; Oh and Liou, 1998). Therefore, taking minor differences of effective bulk compositions in each domain into consideration, an identical retrograde path with a decrease in both P and T conditions can explain the complex varieties in texture and composition of the amphiboles in the eclogites. The barroisites and glaucophanes are bounded by sharp contacts against the actinolite rinds, suggesting that both P and T conditions decreased, without the low-P/T type overprinting, during the later substage of the retrograde metamorphism.

At this stage, chlorite, stilpnomelane, and actinolite formed in rims and cracks of garnets and omphacites. Most rutiles are rimmed by titanites. These modifications also result from hydration reactions under greenschist-facies conditions. Finally, the foliation of eclogites are cut by the Ep + Cal + Qtz or Prh + Qtz veinlets. This textural relation and the stability of prehnite indicate that the eclogites reached P-T conditions less than 280°C at 0.2 GPa in the latest substage of the retrograde metamorphism. Integrating these relations allows us to delineate a possible P-T path for the Chagan-Uzun eclogite, which is a counterclockwise hairpin curve, as shown in Figure 8.

On the other hand, the Chagan-Uzun garnet-amphibolites and the Kurai metabasites contain garnets and barroisites with progressive normal zoning, although they preserve less information to estimate P-T conditions of their prograde stage. The glau-

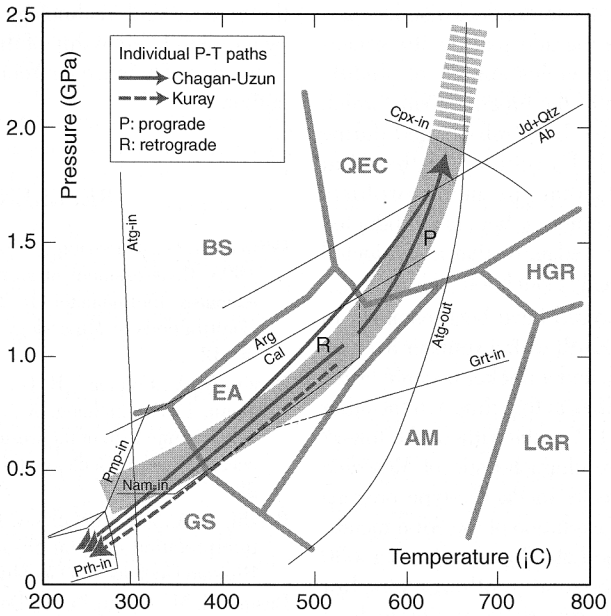

FIG. 8. Pressure-temperature diagram showing the Altai metamorphic facies series (thick shaded line) and individual pressure-temperature paths for the higher-grade metabasites from Chagan-Uzun (arrows with solid lines) and Kurai (arrow with dashed line), with a petrogenetic grid for common metabasites (Oh and Liou, 1998). Reaction curves of Atg-in, Atg-out, Cpx-in, Grt-in, and Nam-in are after Evans et al. (1976), Wunder and Schreyer (1997), Liu et al. (1996), Poli (1993), and Maresch (1977), respectively, and those of Pmp-in and Prh-in are from the petrogenetic grid for low-grade metabasites by Frey et al. (1991). The others were calculated using the program, THERMOCALC. Abbreviations: BS = blueschist facies; GS = greenschist facies; EA = epidote-amphibolite facies; AM = amphibolite facies; QEC = quartz-eclogite facies; HGR = high-pressure granulite facies; LGR = low-pressure granulite facies. The others are the same as those used in Table 1.

cophanes in type-3 garnet-amphibolites exhibit textures similar to those in the eclogites (Fig. 4D), which suggests that the garnet-amphibolites also underwent similar retrogression to the later substage of the retrograde metamorphism for the eclogites. The replacement of barroisites and hornblendes by actinolites, and the Ep + Cal + Qtz or Prh + Qtz veinlets are recognized not only in the eclogites but also in the higher-grade metabasites, except for the LBS and the ACT metabasites. P-T conditions at this stage would be comparable with those of the peak stage for the ACT metabasites.

As a consequence, P-T histories of the Chagan-Uzun garnet-amphibolites and Kurai HBL, GB, and GH metabasites are characterized by a retrograde path with decreasing P and T conditions; these metabasites would have followed a history similar to that of the eclogites since the later substage of the retrograde metamorphism (Fig. 8). However, the retrograde P-T paths of the Kurai metabasites may have passed through P-T ranges with lower dP/dT than those of the Chagan-Uzun metabasites, because no glaucophane has been confirmed in the Kurai metabasites.

P-T evolution of the Altai metabasites and a subduction-zone geotherm

Estimated metamorphic peak conditions of the Altai metabasites from the Chagan-Uzun and Kurai areas range from 300°C at 0.4 GPa to 660°C at 2.0 GPa with successive P-T increases, corresponding to thermal gradients ranging from about 25°C/km in the lowest to about 11°C/km in the highest P-T conditions. The Altai metamorphic facies series defines a single curve convex toward the temperature axis of the P-T diagram (Fig. 8); this curve is similar to a steady-state P-T path in a subduction zone, where young and hot lithosphere has subducted, according to numerical calculations (e.g., Peacock, 1996). The Chagan-Uzun eclogites record prograde and retro-

grade histories, tracing a counterclockwise hairpin-like P-T path. The retrograde path to the greenschist-facies conditions yields similar or slightly higher dP/dT than that of the prograde path, which occurs where rocks have been refrigerated during exhumation. Such a P-T evolution of the Altai metabasites suggests that the metamorphism occurred in conditions where a hot slab subducted beneath a cool mantle wedge, or that a subducted slab changed continuously from hot to cold.

A hot lithosphere would have been common in the Late Precambrian Earth with a younger average age of subducting plate and a thicker oceanic crust, reflecting mantle activities at that time. On the other hand, the hairpin-like P-T paths without the low-P/T type overprinting are characteristic of Mesozoic HP/LT metamorphic rocks in Pacific-type orogens (Ernst, 1988). The P-T evolution of the Altai metabasites indicates that the Late Precambrian (ca. 630 Ma) Altai subduction-zone geotherm was low enough to give rise to characteristics similar to those of Mesozoic HP/LT metamorphic rocks.

Metamorphic facies series of the HP/LT metamorphic belts, formed by oceanic plate subduction, still constitute useful information to constrain the subduction-zone geotherm at that time and the Earth's thermal history. However, in this case, it is necessary to integrate information about the age of subducting plate, because the Earth's mantle might have episodically activated and lost its heat in the Earth's history (Maruyama, 1994; Maruyama and Liou, 1998).

Acknowledgments

We are deeply indebted to E.D. Ghent, B.F. Windley, S. Johnson, J. G. Liou, and M. L. Leech for their critical reading, improvement of the English, and constructive comments on a previous version of the manuscript. We are grateful to S. Maruyama, S. Omori, and T. Komiya for fruitful discussions. This study was carried out as a part of joint project of the Tokyo Institute of Technology and the Institute of Geology, Russian Academy of Sciences, Novosibirsk. S. Maruyama, A. Ishikawa, A. Utsunomiya, and N. Dobretsov (in 1997), and Y. Kaneko, H. Yamamoto, I. Katayama, and Y. Uchio (in 2000) assisted in the field mapping, and the staff of the Institute of Geology, Novosibirsk, helped us during the field work. This study was financially supported in part by a project on Whole Earth Dynamics from the Science and Technology Agency of Japan, and by a research fellowship of the Japan Society for the Promotion of Science for Young Scientists to the first author.

REFERENCES

Berman, R. G., Aranovich, L., Ya. and Pattison, D. R. M., 1995, Reassessment of garnet-clinopyroxene Fe-Mg exchange thermometer: II. Thermodynamic analysis: Contributions to Mineralogy and Petrology, v. 119, p. 30–42.

Berzin, N. A., Coleman, R. G., Dobretsov, N. L., Zonenshain, L. P., Xuchang, X., and Chang, E. Z., 1994, Geodynamic map of the western part of the Paleoasian ocean: Russian Geology and Geophysics, v. 35, p. 5–22.

Berzin, N. A., and Kungurtsev, L. V., 1996. Geodynamic interpretation of Altai-Sayan geological complexes: Russian Geology and Geophysics, v. 37, p. 56–73.

Buslov, M. M., Berzin, N. A., Dobretsov, N. L., and Simonov, V. A., 1993, Geology and tectonics of the Gorny Altai: Guidebook for post-symposium excursion, The 4th International Symposium of the IGCP Project 283 "Geodynamic Evolution of the Paleoasian Ocean": Novosibirsk, Russia: Russian Academy of Sciences, Siberian Section, United Institute of Geology, Geophysics, and Mineralogy.

Buslov, M. M., Saphonova, I.Yu., Watanabe, T., Obut, O. T., Fujiwara, Y., Iwata, K., Semakov, N. N., Sugai, Y., Smirnova, L. V., Kazansky, A. Yu. and Itaya, T., 2001, Evolution of the Paleo-Asian Ocean (Altai-Sayan Region, Central Asia) and collision of possible Gondwana-derived terranes with the southern marginal part of the Siberian continent: Geoscience Journal, v. 5, p. 203–224.

Buslov, M. M. and Watanabe, T., 1996, Intrasubduction collision and its role in the evolution of an accretionary wedge: The Kurai zone of Gorny Altai, Central Asia: Russian Geology and Geophysics, v. 36, p. 83–94.

Dale, J., Holland, T. J. B., and Powell, R., 2000, Hornblende-garnet-plagioclase thermobarometry: A natural assemblage calibration of the thermodynamics of hornblende: Contributions to Mineralogy and Petrology, v. 140, p. 353–362.

Dobretsov, N. L., and Sobolev, N. V., 1984, Glaucophane schists and eclogites in the folded systems of northern Asia: Ofioliti, v. 9, p. 401–424.

Dobretsov, N. L., Berzin, N. A., and Buslov, M. M., 1995, Opening and tectonic evolution of the Paleo-Asian ocean: International Geology Review, v. 35, p. 335–360.

Ernst, W. G., 1972, Occurrence and mineralogic evolution of blueschist belts with time: American Journal of Science, v. 272, p. 657–668.

_____, 1988, Tectonic history of subductionzones inferred from retrograde blueschist P-T paths: Geology, v. 16, p. 1081–1084.

Ernst, W. G., and Liu, J., 1998, Experimental phase-equilibrium study of Al- and Ti-contents of calcic amphibole in MORB—A semiquantitative thermobarometer: American Mineralogist, v. 83, p. 952–969.

Evans, B. W., 1990, Phase relations of epidote-blueschists: Lithos, v. 25, p. 3–23.

Evans, B. W., Johannes, W., Otterdoom, H., and Trommsdorff, V., 1976, Stability of chrysotile and antigorite in the serpentine multisystem: Schweizerische Mineralogische und Petrographische Mitteilungen, v. 56, p. 79–93.

Frey, M., de Capitani, C., and Liou, J. G., 1991, A new petrogenetic grid for low-grade metabasites: Journal of Metamorphic Petrology, v. 9, p. 497–509.

Gaggero, L., and Cortesogno, L., 1997, Data report: Metamorphic mineralogy of Leg 153 gabbros, *in* Karson, J. A., Cannat, M., Miller, D. J., and Elthon, D., eds., Proceedings of the Ocean Drilling Program, Scientific Results, v. 153, p. 531–546.

Graham, C. M., and Powell, R., 1984, A garnet-hornblende geothermometer: Calibration, testing, and application to the Pelona schist, southern California: Journal of Metamorphic Geology, v. 2, p. 13–21.

Hirajima, T., 1996, Effect of jadeite-content on the garnet-clinopyroxene geothermometer for an ultrahigh-pressure eclogite complex: Proceedings of the Japan Academy, v. B72, p. 208–213.

Holland, T. J. B., 1989, The dependence of entropy on volume for silicate and oxide minerals: A review and a predictive model: American Mineralogist, v. 74, p. 5–13.

Holland, T. J. B., and Powell, R., 1998, An internally-consistent thermodynamic dataset for phases of petrological interest: Journal of Metamorphic Geology, v. 16, p. 309–344.

Holland, T. J. B., Baker, J., and Powell, R., 1998, Mixing properties and activity-composition relationships of chlorites in the system MgO-Al_2O_3-SiO_2-H_2O: European Journal of Mineralogy, v. 10, p. 395–406.

Kretz, R., 1983, Symbols for rock-forming minerals: American Mineralogist, v. 68, p. 277–279

Krogh Ravna, E. J., 2000, The garnet-clinopyroxene Fe^{2+}-Mg geothermometer: An updated calibration: Journal of Metamorphic Geology, v. 18, p. 211–219.

Leake, B. E., Woolley, A. R., Arps, C. E. S., Birch, W. D., Gilbert, M. C., Grice, J. D., Hawthorne, F. C., Kato, A., Kisch, H. J., Krivovichev, V. G., Linthout, K., Laird, J., Mandarino, J. A., Maresch, W. V., Nickel, E. H., Rock, N. M. S., Schumacher, J. C., Smith, D. C., Stephenson, N. C. N., Ungaretti, L., Whittaker, E. J. W. and Youzhi, G., 1997, Nomenclature of amphiboles: Report of the subcommittee on amphiboles of the International Mineralogical Association, commission on new minerals and mineral names: American Mineralogist, v. 82, p. 1019–1037.

Liou, J. G., Maruyama, S., and Cho, M., 1987, Very low-grade metamorphism of volcanic and volcaniclastic rocks — mineral assemblages and mineral facies, *in* Frey, M., ed., Low temperature metamorphism: Glasgow, UK, Blackie and Sons Limited, p. 59–113.

Liou, J. G., Maruyama, S., Wang, X., and Graham, S., 1990, Precambrian blueschist terranes of the world: Tectonophysics, v. 181, p. 97–111.

Liu, J., Bohlen, S. R. and Ernst, W. G., 1996, Stability of hydrous phases in subducting oceanic crust: Earth and Planetary Science Letters, v. 143, p. 161–171.

Maresch, W. V., 1977, Experimental studies on glaucophane: An analysis of present knowledge: Tectonophysics, v. 43, p. 109–125.

Maruyama, S., 1994, Plume tectonics: Journal of the Geological Society of Japan, v. 100, p. 24–49.

Maruyama, S., and Liou, J. G., 1998, Initiation of UHP metamorphism and its significance on the Proterozoic/Phanerozoic boundary: The Island Arc, v. 7, p. 6–35.

Oh, C. W., and Liou, J. G., 1998, A petrogenetic grid for eclogite and related facies under high-pressure metamorphism: The Island Arc, v. 7, p. 36–51.

Peacock, S. M., 1996, Thermal and petrologic structure of subduction zone, *in* Bebout, G. E., Scholl, D. W., Kirby, S. H., and Platt, J. P., eds., Subduction: Top to bottom: American Geophysical Union, Geophysical Monograph, v. 96, p.119–133.

Poli, S., 1993, The amphibolite-eclogite transformation: An experimental study on basalt: American Journal of Science, v. 293, p. 1061–1107.

Powell, R., and Holland, T. J. B., 1994, Optimal geothermometry and geobarometry: American Mineralogist, v. 79, p. 120–133.

Sengör, A. M. C., Natal'in, B. A., and Burtman, V. S., 1994, Tectonic evolution of Altaides: Russian Geology and Geophysics, v. 35, p. 33–47.

Simonov, V. A., Dobretsov, N. L. and Buslov, M. M., 1994, Boninite series in structures of the Paleo-Asian ocean: Russian Geology and Geophysics, v. 35, p. 182–199.

Sobolev, V. S., Dobretsov, N. L., Bakilov, A. B., and Shatsky, V. S., 1986, Eclogites from various type of metamorphic complexes in the USSR and the problem of their origin, *in* Evans, B. W., and Brown, E. H., eds., Blueschists and eclogites: Geological Society of America Memoir, v. 164, p. 349–364.

Toriumi, M., 1975, Petrological study of the Sanbagawa metamorphic rocks, Kanto Mountains, central Japan: University of Tokyo Bulletin, University Museum, v. 9. p. 1–99.

Tropper, P., Manning, C. E., Essene, E. J., and Kao, L. S., 2000, The compositional variation of synthetic sodic amphiboles at high and ultra-high pressures: Contributions to Mineralogy and Petrology, v. 139, p. 146–162.

Werner, C. D., 1997, Geochemistry of rocks and minerals of the gabbro complex from the Mark area, *in* Karson, J. A., Cannat, M., Miller, D. J. and Elthon, D., eds., Proceedings of the Ocean Drilling Program, Scientific Results, v. 153, p. 491–504.

Wunder, B., and Schreyer, W., 1997, Antigorite: High-pressure stability in the system MgO-SiO_2-H_2O (MSH): Lithos, v. 41, p. 213–227.

Yokoyama, K., Brothers, R. N., and Black, P. M., 1986, Regional eclogite facies in the high-pressure metamorphic belt of New Caledonia, *in* Evans, B. W., and Brown, E. H., eds., Blueschists and eclogites: Geological Society of America Memoir, v. 164, p. 407–423.

Zonenshain, L. P., Kuzmin, M. I., and Natapov, L. M., 1990, Geology of the USSR: A plate tectonic synthesis: Washington, DC, American Geophysical Union, Geodynamic Monograph .